Magnitude of the carbon isotope excursion at the Paleocene-Eocene Thermal Maximum: The role of plant community change

Francesca A. Smith, Scott L. Wing, Katherine H. Freeman

PII: S0012-821X(07)00444-X
DOI: doi: 10.1016/j.epsl.2007.07.021
Reference: EPSL 8812

To appear in: *Earth and Planetary Science Letters*

Received date: 7 October 2006
Revised date: 3 July 2007
Accepted date: 3 July 2007

Please cite this article as: Francesca A. Smith, Scott L. Wing, Katherine H. Freeman, Magnitude of the carbon isotope excursion at the Paleocene-Eocene Thermal Maximum: The role of plant community change, *Earth and Planetary Science Letters* (2007), doi: 10.1016/j.epsl.2007.07.021

Magnitude of the carbon isotope excursion at the Paleocene-Eocene Thermal Maximum: The role of plant community change

Francesca A. Smith[1,2*], Scott L. Wing[1], Katherine H. Freeman[2]

[1] Department of Paleobiology, National Museum of Natural History, Smithsonian Institution, Washington, DC 20560, USA
[2] Department of Geosciences, Pennsylvania State University, University Park, PA 16802, USA
* Corresponding author. Current address: Department of Earth and Planetary Sciences, Northwestern University, 1850 Campus Drive, Evanston, IL 60208; Phone (847) 491-3459, Fax (847) 491-8060, cesca@earth.northwestern.edu

ABSTRACT

Carbon-isotope measurements ($\delta^{13}C$) of leaf-wax *n*-alkanes from the Paleocene-Eocene Thermal Maximum (PETM) in the Bighorn Basin, Wyoming reveal a negative carbon isotope excursion (CIE) of 4-5‰, which is 1-2‰ larger than that observed in marine carbonate $\delta^{13}C$ records. Reconciling these records requires either that marine carbonates fail to record the full magnitude of the CIE or that the CIE in plants has been amplified relative to the marine. Amplification of the CIE has been proposed to result from an increase in available moisture that allowed terrestrial plants to increase ^{13}C-discrimination during the PETM. Leaf physiognomy, paleopedology and hydrogen isotope ratios of leaf-wax lipids from the Bighorn Basin, however, all suggest that rather than a simple increase in available moisture, climate alternated between wet and dry during the PETM. Here we consider two other explanations and test them quantitatively with the carbon isotopic record of plant lipids. The "marine modification" hypothesis is that the marine carbonate record was modified by chemical changes at the PETM and that plant lipids record the true magnitude of the CIE. Using atmospheric CO_2 $\delta^{13}C$ values estimated from the lipid record, and equilibrium fractionation between CO_2 and carbonate, we estimate the expected CIE for planktonic foraminifera to be 6‰. Instead,

the largest excursion observed is about 4‰. No mechanism for altering marine carbonate by 2‰ has been identified and we thus reject this explanation. The "plant community change" hypothesis is that major changes in floral composition during the PETM amplified the CIE observed in n-alkanes by 1-2‰ relative to marine carbonate. This effect could have been caused by a rapid transition from a mixed angiosperm/conifer flora to a purely angiosperm flora. The plant community change hypothesis is consistent with both the magnitude and pattern of CIE amplification among the different *n*-alkanes, and with data from fossil plants. This hypothesis predicts that the magnitude and pattern of amplification of CIEs among different *n*-alkanes will vary regionally and systematically depending on the extent of the replacement of conifers by angiosperms during the PETM.

Keywords: *n*-alkanes, plant lipids, carbon isotopes, hydrogen isotopes, Paleocene-Eocene Thermal Maximum, global warming

1. INTRODUCTION

The Paleocene-Eocene Thermal Maximum (PETM) was a period of abrupt (~10 kyr onset), extreme (4-8˚C) and short-lived (100-200 kyr) warming that occurred about 55.8 million years ago (Farley and Eltgroth, 2003; Fricke and Wing, 2004; Kennett and Stott, 1991; Koch et al., 1992; Rohl et al., 2000; Sluijs et al., 2006; Zachos et al., 2006; Zachos et al., 2003) and significantly altered terrestrial and marine ecosystems. During this warming, the composition of plant communities in the Bighorn Basin, Wyoming changed radically, though largely transiently, partly by the immigration of species

formerly found only at lower latitudes (Wing et al., 2005). Vegetation in the Arctic also changed, as demonstrated by a temporary rise in angiosperm pollen and decline in gymnosperm and fern palynomorphs (Sluijs et al., 2006). Vertebrate faunas were strongly affected by immigrations that led to changes in taxonomic and trophic structure of communities and the appearance of modern mammals in North America (Beard and Dawson, 1999; Clyde and Gingerich, 1998; Gingerich, 2003). In the marine realm, the PETM is associated with a mass extinction of benthic foraminifera (Thomas, 1998), change in the composition, distribution and evolutionary rates of marine plankton (Crouch et al., 2001; Gibbs et al., 2006; Kelly, 2002), and profound ocean acidification (Zachos et al., 2005).

The PETM is marked by a large negative carbon isotope excursion (CIE) in terrestrial and marine carbonates and organic matter (Kennett and Stott, 1991; Koch et al., 1995; Koch et al., 1992; Magioncalda et al., 2004; Wing et al., 2005), reflecting a rapid release of ^{13}C-depleted carbon into the ocean-atmosphere system. Several carbon sources have been proposed, including methane clathrates (Dickens et al., 1995), burning of peat and coal (Kurtz et al., 2003), volatile-rich comet (Kent et al., 2003), thermogenic methane (Svensen et al., 2004) and organic matter oxidation due to uplift of epicontinental seas (Higgins and Schrag, 2006). Shoaling of the lysocline in the global ocean, as indicated by dissolution of calcium carbonate in marine sediments, indicates the mass of carbon released was at least 4500 Gt (Zachos et al., 2005). This amount of carbon is comparable to the amount that would be released by burning the entire fossil fuel resource base (Metz et al., 2001).

Carbon in the ocean and atmosphere is well mixed on the time scale of the onset

77 of the PETM (~10 kyr), and in theory, biosphere signatures of this event would reveal an
78 identical and synchronous CIE. However, marine and terrestrial proxies present us with
79 distinct signatures across this interval of time. Specifically, the magnitude of the
80 negative carbon isotope excursion at the Paleocene-Eocene boundary recorded in
81 terrestrial reservoirs is significantly larger than in marine reservoirs: ~6-8 ‰ in paleosol
82 carbonates (Bowen et al., 2001; Koch et al., 1995; Schmitz and Pujalte, 2003) compared
83 with ~2.5-4 ‰ in marine carbonates (Bains et al., 1999; Kennett and Stott, 1991; Thomas
84 et al., 2002; Tripati and Elderfield, 2004; Zachos et al., 2003). The cause for the >3 ‰
85 difference in terrestrial and marine carbonates has been explored by considering the
86 effects of warming and elevated atmospheric CO_2 on ocean chemistry, soil processes and
87 carbon isotope discrimination by plants (Bowen et al., 2004). Acidification of the oceans
88 and the associated decrease in $[CO_3^{2-}]$ from the addition of CO_2 could have reduced the
89 amplitude of the marine CIE by ~0.5 ‰. Increased C-input and soil turnover could have
90 increased the magnitude of the terrestrial CIE by 0.8‰. Bowen et al. (2004) suggested
91 that the remaining 1.7‰ was caused by greater discrimination against ^{13}C by plants
92 during the PETM as the result of a postulated increase in water availability.
93 Wetter PETM conditions have been inferred from increases in kaolinitic clays in
94 shallow marine sediments of the Tethys, Atlantic and Southern Oceans, possibly
95 reflecting higher rates of chemical weathering (Bolle and Adatte, 2001; Cramer et al.,
96 1999; Gibson et al., 2000; Robert and Kennett, 1994). Increases in terrestrial
97 palynomorphs in nearshore marine deposits in New Zealand also have been interpreted as
98 indicating higher runoff during the PETM (Crouch et al., 2003). In contrast, other
99 evidence favors a drier, or more seasonally dry, climate during the PETM. Schmitz and

Pujalte (2003) observed sedimentological changes in northern Spain indicating flashy deposition and highly seasonal precipitation during the PETM. General circulation models (GCMs) suggest latitudinal variability in changes in precipitation, with an increase in total precipitation over continents at higher latitudes and in areas of monsoonal climate (Huber and Sloan, 1999; Shellito et al., 2003). However, GCM results for specific regions disagree, with one showing decreased (Huber and Sloan, 1999) and another showing increased (Shellito et al., 2003) summer precipitation over interior North America during the PETM. Fossil floras from the Bighorn Basin, WY, suggest that precipitation first decreased and then increased during the PETM (Wing et al., 2005). The chemical composition and morphology of paleosols shows even more variability in precipitation, revealing four cycles of wetter and drier conditions during the PETM in the Bighorn Basin (Kraus and Riggins, 2007). Based on these records, the hypothesized increase in ^{13}C-discrimination by plants should not be attributed to a simple increase in water availability in the Bighorn Basin.

Here we consider two hypotheses for reconciling the terrestrial and marine CIEs. The "marine modification" hypothesis is that marine carbonates fail to record the full magnitude of the CIE, and that the excursion seen in terrestrial leaf waxes is the same magnitude as that in the atmosphere and ocean (Pagani et al., 2006). The "plant community change" hypothesis is that the CIE recorded in continental carbon isotope records is larger than the atmosphere-ocean excursion because, in the regions studied, the plants that dominated terrestrial vegetation during the PETM discriminated against ^{13}C more than those that were dominant immediately before and after the event. We evaluate the competing hypotheses using carbon and hydrogen isotope ratios of high-molecular

123 weight (C_{25}-C_{33}), odd-carbon-numbered *n*-alkanes that are constituents of leaf waxes
124 (Eglinton and Hamilton, 1967) and are widely used as a diagnostic biomarker for
125 vascular plants in sedimentary systems (Freeman and Colarusso, 2001; Pagani et al.,
126 2006; Schouten et al., 2007).
127
128 **2. METHODS**
129 **2.1 Study area**
130 The Cabin Fork study area is located in the southeastern Bighorn Basin of
131 Wyoming (Figure 1). The Paleocene-Eocene transition is recorded in the lowest
132 Willwood Formation. Locally the underlying Fort Union Formation is about 110 m
133 thick, rests unconformably on Cretaceous strata, and consists of gray to grayish-yellow
134 mudstones, carbonaceous shales (3-40% TOC), mostly fine-grained sandstones, and rare
135 coals near its base (Bown, 1980; Wing, 1998). The mudstones, shales and coal represent
136 deposition on low-lying floodplains, and the sandstones have bedding features and
137 geometries consistent with deposition in fluvial channels or channel margins. Fossil
138 plants and mammals show that all of the Fort Union Formation in the study area is late
139 Paleocene in age (Wing, 1998; Wing et al., 2005). About 120 m of the lowest Willwood
140 Formation is exposed in the Cabin Fork drainage and adjacent areas, and it is composed
141 of pale, variegated red, purple and yellow mudstones, rare lenticular carbonaceous shales,
142 and fine-grained sandstones (Bown, 1980; Wing, 1998). The variegated mudstones
143 represent paleosols formed on fine, overbank deposits; the lenticular shale bodies were
144 deposited in abandoned channels; and the sandstones represent channel or channel-
145 margin settings (Bown, 1980; Wing, 1998).

146 The PETM is represented by a ~40 m-thick interval of strata at the base of the
147 Willwood Formation. The carbon isotope excursion that typifies the PETM is recorded
148 in both bulk organic matter and individual *n*-alkanes contained in mudstone paleosols
149 (Figure 2). Fossil mammals demonstrate the characteristic succession of biozones (Cf3-
150 Wa0-Wa1) that is associated with the PETM in Wyoming (Bloch et al., 2004; Gingerich,
151 2003; Wing et al., 2005).

152 PETM-age rocks crop out extensively in the study area and dip shallowly to the
153 west, parallel to topography. Sections were measured with a Jacob's staff and sighting
154 level and correlated by tracing beds with a differential GPS with sub-meter precision and
155 employing a geometric model of local structure following methods outlined by Gingerich
156 (2001) . (DGPS and geometric model by D. Boyer.)
157

158 **2.2 Sample collection and cleaning**

159 Samples were collected from outcrops by removing weathered surface material to
160 expose fresh, well-consolidated rock. Blocks 10-15 cm across were collected in cloth
161 sample bags and allowed to air dry. In the laboratory, the surfaces of the blocks were
162 cleaned by grinding off the outer 1-2 mm with a dremel tool using a solvent-rinsed
163 tungsten carbide bit. Each sample was then rinsed with dichloromethane. Samples were
164 further dried in a 70˚C oven overnight and then pulverized in a ball mill that was cleaned
165 between samples with ashed quartz sand, distilled water, methanol, and dichloromethane.
166

167 **2.3 *n*-Alkane extraction characterization and isotope measurements**

Lipids were Soxhlet extracted from 50-70 g of pulverized sediment with a dichloromethane:methanol azeotrope (9:1, v/v) for 24 hours. Total lipid extracts were concentrated by rotoevaporation, and then separated into compound classes by polarity using short columns filled with approximately 3 g of activated silica gel (70-230 mesh). The hydrocarbon fraction was eluted using hexane (4 mL); polar compounds were eluted using dichloromethane/methanol (1/1, v/v) and archived. *n*-Alkanes were identified through mass spectra, molecular ion mass, retention time and comparison with standards ("Mixture A" from A. Schimmelmann) using an Agilent 6890 gas chromatograph coupled to an Agilent 5972 quadrupole mass spectrometer. The GC program was started at 60 ˚C (held for 1 minute) and increased to 320˚C at 6˚C/minute, and was subsequently held at 320 ˚C for 20 minutes.

Carbon-isotope ratios of individual *n*-alkanes were measured on a Thermo Finnigan Delta Plus XP with a Gas Chromatograph and Combustion interface (GCC). Hydrogen isotope ratios were measured with a gas chromatograph and high temperature pyrolysis furnace (1400˚C) interface (Burgoyne and Hayes, 1998; Hilkert et al., 1999). For both measurements, the GC was programmed from 60 ˚C (held for 1 minute) to 170 ˚C at 15 ˚C/minute and then to 320 ˚C at 5 ˚C/minute, and held for 20 minutes. Isotope values for both carbon and hydrogen were calculated relative to co-injected standards and are reported relative to VPDB for carbon and VSMOW for hydrogen isotope ratios. The standard solution contained androstane ($\delta^{13}C$ = –28.47 ‰; δD = –256.4 ‰), squalane ($\delta^{13}C$ = –20.36 ‰; δD = –169.9 ‰) and C_{41} *n*-alkane ($\delta^{13}C$ = –28.84 ‰; δD = –205.7 ‰). (Standard measurement by off-line preparation and dual-inlet isotope-ratio mass spectrometry by A. Schimmelmann.)

Carbon isotope ratios for *n*-alkanes were determined relative to androstane and samples were run in duplicate; standard deviations of replicate runs are reported in Table 1. The average value for co-injected *n*-C_{41} standard was -28.73 ± 0.24 ‰ (± S.D.; n=17). The precision for $\delta^{13}C$ measurements is ± 0.25 ‰ or better.

The H_3^+ factor was measured daily and the average was 4.971 ± 0.085 ppm (± S.D.) (Sessions et al., 2001). Hydrogen isotope ratios were calculated relative to the *n*-C_{41} standard peak to avoid co-elution. Each sample was run at least twice and the standard deviation of replicate measurements of *n*-C_{29} from samples was less than 1.5‰ (Table 1). The average values for co-injected androstane and squalane were -253 ± 3 and -162 ± 4 ‰ (± S.D.; n=15). We determined instrument performance daily by measuring a suite of C_{16} to C_{30} n-alkanes ("Mixture A" from A. Schimmelmann) with a co-injected standard with *n*-C_{14}, androstane, squalane and *n*-C_{41}. The standard deviation for replicate measurements ranges from 0.8 to 5.3 ‰ with an average standard deviation of 2.1 ‰ for 7 measurements of the 15 n-alkanes in Mixture A. An estimate of overall analytical precision is ± 5 ‰ or better.

2.4 Estimated abundance of major plant groups

We quantified the relative abundance of major plant groups at 96 fossil localities spanning the latest Paleocene and earliest Eocene in the Bighorn Basin (65 Paleocene, 5 PETM, 26 post-PETM early Eocene). Individual localities generally are excavations less than 2 by 3 meters horizontally and less than half a meter in stratigraphic thickness. The plant-bearing rock is claystone to very fine sandstone and represents deposition in fluvial environments including abandoned channel fills, floodplain backswamps, levees,

214 crevasse splays and point bars. The fine grain size indicates low-energy deposition and
215 therefore the leaf fossils are likely to represent localized samples of floodplain
216 vegetation.

217 Previous work demonstrates a high correlation between foliar area and stem basal
218 area for trees (Burnham et al., 1992), so leaf fossils were used to estimate biomass of
219 major groups of plants in the Paleocene-Eocene forests. For each locality all identifiable
220 leaf fragments with greater than 50% of their area preserved were assigned to a major
221 taxonomic group: pteridophytes (ferns and horsetails), ginkgos, conifers,
222 monocotyledonous angiosperms, or dicotyledonous angiosperms. For bedding surfaces
223 covered with conifer needles the number was estimated based on density and area from a
224 standard counted region.

225

226 **3. RESULTS**

227 **3.1 Leaf-wax lipids**

228 Hydrocarbons extracted from Cabin Fork sediments are nearly exclusively high-
229 molecular weight (C_{23}-C_{33}) *n*-alkanes with a strong odd-over-even predominance,
230 demonstrating that they are derived from vascular plants (Eglinton and Hamilton, 1967).
231 The most abundant chain-length was either *n*-C_{29} or *n*-C_{31} (Figure 3).

232 Carbon-isotope ratios of individual *n*-alkanes range from -29.2 ‰ to -37.4 ‰ and
233 generally become more negative with increasing chain length within a sample (Table 1,
234 Figure 2). Progressively more ^{13}C-depleted values with increasing chain length are also
235 observed in many modern plants, particularly dicotyledenous angiosperms (Bi et al.,
236 2005; Chikaraishi and Naraoka, 2003; Collister et al., 1994).

All *n*-alkanes show a marked negative carbon isotope excursion beginning at -0.85 m and persisting to 37.3 m (Table 1, Figure 2). The magnitude of the negative shift between the samples at -13.75 m and -0.85 m is 4.0 ‰ for C_{25}, 3.7 ‰ for C_{27}, 4.4 ‰ for C_{29}, and 5.1 ‰ for C_{31}. Hydrogen-isotope ratios of C_{29} *n*-alkane range from -183 to -197 ‰ (Table 1). The onset of the PETM is marked by a +13 ‰ shift followed by a -14 ‰ shift within the lower PETM (Figure 2).

The average chain-length (ACL) was calculated from total ion chromatograms as the peak-area weighted average chain-length using the C_{25}, C_{27}, C_{29}, C_{31}, and C_{33} *n*-alkanes (Eglinton and Hamilton, 1967).

$$ACL = (25A_{25}+27A_{27}+29A_{29}+31A_{31}+33A_{33})/(A_{25}+A_{27}+A_{29}+A_{31}+A_{33}) \quad (1)$$

A is the area under the chromatographic peak for each *n*-alkane (Figure 3). Average chain length increases across the PETM from a pre-PETM average of 28.6 (lowest two samples) to 30.1 for the lowest PETM sample at -0.85 m. The maximum ACL of 30.6 is observed at 8.2 m.

3.2 Fossil plants

A total of 30,153 leaves were counted: 21,793 from the latest Paleocene, 1,995 from the PETM, and 6,365 from the earliest post-PETM Eocene. The mean number of leaves per locality was 309 (standard deviation=631). The numbers and proportions of leaves for each major plant group are given for each of the three time periods in Table 2.

The Paleocene and post-PETM Eocene collections are dominated numerically by leaves of conifers (~75%), which are almost exclusively of just two genera in the family Taxodiaceae, *Glyptostrobus* and *Metasequoia*. Nearly all the remaining leaves from these sites are dicotyledonous angiosperms belonging to a number of families, most prominently Betulaceae. In contrast, conifers are absent from all five PETM localities, and the dicot leaves that dominate them belong to genera and families (especially Fabaceae) that are rare before and after the PETM.

In living forest floor litter, the total leaf area for each species is strongly positively correlated with its stem cross-sectional area in the local forest (Burnham et al., 1992). The number of leaves is less highly correlated with stem area because species with small leaves produce an appropriate amount of photosynthetic area by having more leaves. Leaves of *Glyptostrobus* and *Metasequoia* average about 5% of the area of the dicots they occur with. Therefore, the numerical dominance of conifers before and after the PETM almost certainly overestimates their true abundance in the vegetation. To better approximate relative biomass for the fossil forest, the number of conifer leaves should be divided by a factor of 20. The adjusted percent of conifers for the latest Paleocene and earliest post-PETM time is 13-14%, assuming that conifer and dicot leaves have equal preservation potential.

4. DISCUSSION

4.1 Carbon-isotope excursions in terrestrial reservoirs

The negative carbon isotope excursion recorded in leaf-wax *n*-alkanes ranges from 3.7 ‰ to 5.1 ‰, ~1-2 ‰ greater than for the associated bulk organic matter (~3‰)

282 from the same samples (Figure 2) (Wing et al., 2005). The bulk organic matter CIE for
283 the Cabin Fork area is the same magnitude as that observed in other bulk organic matter
284 records from the northern Bighorn Basin (Polecat Bench) (Magioncalda et al., 2004).
285 Bulk soil organic matter is subjected to substantial transformation, selective preservation
286 and degradation during pedogenesis, which could have dampened its record of the
287 isotope excursion. Plant waxes are more resistant to diagenetic alteration than many
288 components of bulk organic matter and we suggest they more faithfully record the
289 isotopic composition of ancient vegetation.

290 The magnitude of the isotope excursion observed in soil carbonates from the
291 Bighorn Basin ranges from 6 to 8‰ (Bowen et al., 2001; Koch et al., 1995), which is 1-4
292 ‰ larger than in the leaf waxes. Soil carbonates incorporate carbon isotopic signatures
293 of a mixture of atmospheric and respired CO_2, and the amplification of the CIE in soil
294 carbonates relative to the plant lipid CIE could reflect a greater contribution of carbon
295 from SOM to nodule formation during the PETM (Bowen et al., 2004; Cerling, 1984).
296 For this to be the case, the rate of organic matter turnover would have had to increase in
297 order to overcome the enhanced contribution of atmospheric CO_2 due to the postulated
298 increase in atmospheric pCO_2 (Zachos et al., 2003). Faster rates of soil organic matter
299 turnover fueled by the warmer climate could have driven this amplification of the soil
300 carbonate CIE relative to plant matter (Bowen et al., 2004).

301 The negative carbon isotope excursion in plant wax *n*-alkanes measured in the
302 Bighorn Basin (~4-5‰, depending on the chain length) is comparable to that observed in
303 *n*-alkanes from sediment from Walvis ridge in the southern Atlantic Ocean (~4-5‰)
304 (Hasegawa et al., 2006), about 1‰ smaller than observed for *n*-alkanes from Arctic

305 Ocean sediments (~5-6‰) (Pagani et al., 2006), and 1-2‰ larger than *n*-alkanes from
306 New Zealand (~3‰) (Kaiho et al., 1996). Comparison of these records suggest that the
307 magnitude of the carbon isotope excursion recorded in *n*-alkanes varies regionally.
308
309 **4.2 ^{13}C-Discrimination by plants**
310 Carbon isotope discrimination is a measure of the difference between the carbon
311 isotope ratio of atmospheric CO_2 and the plant and is defined as:
312
313 $$\Delta = (R_a/R_p - 1) \times 1000 = (\delta^{13}C_a - \delta^{13}C_p)/(1+ \delta^{13}C_p/1000) \cong \delta^{13}C_a - \delta^{13}C_p \quad (2)$$
314
315 where R represents the $^{13}C/^{12}C$ ratio and $\delta^{13}C$ refers to the carbon isotope abundance of
316 the atmosphere (a) and plant (p), where $\delta^{13}C = (R_{sample}/R_{standard} - 1) \times 1000$ (Farquhar et
317 al., 1989). Delta values are expressed relative to a standard (VPDB) in permil (‰).
318 To estimate carbon isotope discrimination by plants across the PETM, we
319 compare *n*-alkane $\delta^{13}C$ records to values for atmospheric CO_2 estimated from marine
320 records. Because fine-scale correlation of marine and terrestrial sediments across the
321 PETM is difficult, we divided the Paleocene-Eocene boundary sediments into four
322 intervals: pre-CIE, peak CIE, recovery and post-CIE (Tables 3 and 4). The carbon
323 isotope ratio of atmospheric CO_2 ($\delta^{13}C_{Atm}$) for each interval is estimated from planktonic
324 foraminifera carbon isotope ($\delta^{13}C_{pf}$) records from ODP Site 690 from Maud Rise in the
325 Southern Ocean (Thomas et al., 2002) and ODP Site 1209 from Shatsky Rise in the
326 tropical North Pacific (Zachos et al., 2003). The $\delta^{13}C_{Atm}$ values are calculated from
327 $\delta^{13}C_{pf}$ by assuming isotopic equilibrium between the atmosphere, marine dissolved

328 inorganic carbon (DIC) and the calcite of planktonic foraminifera (Freeman and Pagani,
329 2005; Koch et al., 1992), using the temperature-sensitive equilibrium fractionation factor
330 between atmospheric CO_2 and calcite from Romanek et al. (1992) (see Table 3).
331 Temperature values are estimated from oxygen isotope ratios ($\delta^{18}O_{pf}$) (Thomas et
332 al., 2002; Zachos et al., 2003) and Mg/Ca ratios of planktonic foraminifera (Tripati and
333 Elderfield, 2004; Zachos et al., 2003) (see Table 3 for calculations). By using two
334 sediment cores and two temperature proxies, we calculate a range of possible values for
335 carbon isotope ratios of atmospheric CO_2 and minimize noise or bias that may be inherent
336 in a single record or temperature proxy (Figure 2B).
337 The $\delta^{13}C_{pf}$ records from Site 690 and Site 1209 show negative carbon isotope
338 excursions of 3.6‰ and 2.7‰ respectively (Table 3). The magnitude of the CIE in the
339 calculated $\delta^{13}C_{Atm}$ values is smaller, ranging from 2.8‰ to 2.2‰ (Table 3), reflecting the
340 decrease in isotopic fractionation between calcite and atmospheric CO_2 at the warmer
341 PETM temperatures. The carbon isotope ratio of total plant tissue ($\delta^{13}C_{TT}$) is calculated
342 by applying an enrichment factor ($\varepsilon_{lipid\text{-}TT} \approx \delta_{lipid} - \delta_{TT}$) of 4.9‰ to the $\delta^{13}C$ values
343 measured for C_{31} *n*-alkanes based on data published for C_3 angiosperms and conifers (Bi
344 et al., 2005; Chikaraishi and Naraoka, 2003; Collister et al., 1994) (Figure 4A, Table 4).
345 Carbon isotope discrimination is calculated from $\delta^{13}C_{TT}$ and $\delta^{13}C_{Atm}$ using equation 2. In
346 all calculated scenarios, net plant discrimination increased between 2.5 ‰ - 3.2 ‰ during
347 the PETM (Figure 4C, Table 4).
348
349
350

4.3 Climate and increased ^{13}C-discrimination

4.3.1 Hydrologic conditions and p_i/p_a ratios

During photosynthesis by C_3 plants, the enzyme-catalyzed uptake of CO_2 by Rubisco discriminates against ^{13}C and the extent of this discrimination depends on the relative flux of CO_2 into and out of the leaf. The net discrimination is sensitive to the ratio between intercellular partial pressure of CO_2 within the leaf (p_i) and the atmospheric partial pressure of CO_2 (p_a):

$$\Delta = a + (b-a) \times p_i/p_a \qquad (3)$$

where a is fractionation caused by diffusion of CO_2 through stomata (4.4‰), b is the fractionation due to carboxylation by Rubisco (27‰) and p_i/p_a is the ratio of CO_2 concentrations inside the leaf (p_i) relative to the atmosphere (p_a) (Farquhar et al., 1989). This ratio is controlled by the stomata and the photosynthetic uptake of CO_2.

When we calculate p_i/p_a ratios from the isotopic results, we find they show a marked increase across the PETM, rising by 11% to 14%. In modern plants, p_i/p_a ratios are largely controlled by water availability, as demonstrated both in the laboratory and in natural ecosystems (Bowling et al., 2002; Edwards et al., 2000). Changes in atmospheric pCO_2 do not appear to affect p_i/p_a or Δ in laboratory experiments over a range from 150 to 1400 ppmv CO_2 (Arens et al., 2000; Beerling and Woodward, 1995; Polley et al., 1993), in herbarium and tree ring samples from the historic rise in pCO_2 (Saurer et al., 2004), or in fossils spanning Pleistocene glacial-interglacial cycles in pCO_2 (Beerling, 1996; Ward et al., 2005). Changes in net plant discrimination observed in the geologic

374 past have been attributed to changes in available moisture (Beerling, 1996; Schouten et
375 al., 2007; Ward et al., 2005), and the increase in Δ and p_i/p_a during the PETM could
376 reflect wetter conditions. However, floral assemblages (Wing et al., 2005) and paleosol
377 properties suggest otherwise (Kraus and Riggins, 2007), and indicate instead cycles of
378 wetting and drying.
379
380 **4.3.2 Paleohydrologic proxy estimates for the PETM**
381 Hydrogen isotope ratios of individual *n*-alkanes reflect changes in available
382 moisture and can help to assess further the hypothesis that wetter conditions led to
383 increased discrimination during the PETM. Leaf-wax lipids from modern plants reflect
384 meteoric water δD values (Chikaraishi and Naraoka, 2003; Sachse et al., 2006; Smith and
385 Freeman, 2006) and the degree of D-enrichment from soil evaporation and transpiration
386 (evaporation through stomata) (Smith and Freeman, 2006). Therefore, if the δD values
387 of meteoric waters are constrained, δD signatures of *n*-alkanes reflect humidity, with
388 drier conditions leading to more positive δD values and vice versa.
389 Fricke et al. (1998) estimated river water $\delta^{18}O$ values from *Coryphodon* tooth
390 enamel ($\delta^{18}O_{cory}$) across the PETM. According to their estimates, the $\delta^{18}O_{river}$ values
391 average -6.8‰ (n=11) before the PETM (Cf-2) and -4.5‰ (n=8) during the PETM (Wa-
392 O). The δD values for surface waters are estimated from $\delta^{18}O_{river}$ values by using the
393 Global Meteoric Water Line relationship ($\delta D = 8\ \delta^{18}O + 10$) (Craig, 1961) and are -44‰
394 for pre-PETM (Cf-2) and -26‰ for the PETM (Wa-0) interval. We caution that the Cf-2
395 biozone from which the $\delta^{18}O_{cory}$ data are derived pre-dates all of the *n*-alkane sample
396 horizons, making direct comparisons impossible. The PETM (Wa-0) tooth enamel

397 samples come from site 83613 on Polecat Bench (Fricke et al., 1998), which is close to
398 the stratigraphic level of Purple-2 (P. Gingerich, pers. comm.) and is therefore in the
399 middle of the carbon isotope excursion (Gingerich, 2001).

400 Expected leaf-wax *n*-alkane δD values can be estimated from these surface water
401 δD values by applying a Craig-Gordon-type leaf water isotope model for transpiration
402 (Craig and Gordon, 1965; Roden and Ehleringer, 1999). This model quantitatively
403 describes the relationship between relative humidity and leaf-wax *n*-alkane δD values and
404 is fully described by Smith and Freeman (2006). Given the estimated surface water δD
405 values, a transpiration corrected $\varepsilon_{lipid\text{-}water}$ value for C_3 plants of -181‰ (Smith and
406 Freeman, 2006), an estimated PETM temperature increase from 20˚C to 25˚C (Fricke and
407 Wing, 2004; Wing et al., 2005) and a constant relative humidity of 60%, the predicted
408 δD_{C29} increases from -205‰ for the pre-PETM (Cf-2) level to -190‰ for the PETM level
409 (Figure 2E: grey square). If relative humidity increased by 25% during the PETM (i.e.
410 'Bowen et al., 2004), the predicted δD_{C29} value for the PETM shifts to -198‰ due to
411 reduced transpiration (Figure 2E: open square). These estimates should not be affected
412 by plant community change at the PETM because, unlike modern grasses (Smith and
413 Freeman, 2006), modern conifers and dicots show similar apparent fractionation factors
414 ($\varepsilon_{lipid\text{-}water}$) (Bi et al., 2005; Chikaraishi and Naraoka, 2003; Sachse et al., 2006).

415 Measured lipid hydrogen isotope ratios shift first to more positive and then to
416 more negative values within PETM, similar to the pattern observed in the Arctic *n*-alkane
417 δD record (Pagani et al., 2006). Although these shifts are difficult to interpret without
418 additional constraints on surface water δD values, they suggest first drier and then wetter
419 conditions within the PETM, which is consistent with changes in the Bighorn Basin in

floral composition, plant physiognomy and paleosol features (Kraus and Riggins, 2007; Wing et al., 2005). The measured δD_{C29} value for the sample closest to the middle of the CIE (Cab1-04-06; -190‰; Table 1) agrees well with the predicted value of -190‰ for constant relative humidity across the PETM (Figure 2E).

Our data are not consistent with a single, large increase in atmospheric moisture, and lend support to the floral and paleosol records that indicate variable hydrologic conditions across the PETM. In addition, the modeled estimate of a 25% increase in available moisture by Bowen et al. (2004) sought to explain a 1.7‰ increase in discrimination. The plant lipid data presented here indicate that the increase was even greater, from 2.5-3.2‰, and would require a 30-35% increase in available moisture based on the model in Bowen et al. (2004). We suggest other or additional factors are needed to understand PETM plant $\delta^{13}C$ signatures as well as to account for the marine-terrestrial CIE difference.

4.3.3 Warming and increased ^{13}C-discrimination

An alternative mechanism for increasing the terrestrial CIE relative to the marine invokes increased plant isotopic discrimination resulting from climate warming. Temperature exerts a significant effect on carbon isotope discrimination, although its effects are often hard to discern in field data due to confounding variables. However, controlled greenhouse experiments demonstrate that increasing temperature leads to greater ^{13}C discrimination (Edwards et al., 2000). For example, the $\delta^{13}C_{cellulose}$-temperature response of bean plants (*Vicia faba)* grown at 18 and 28˚C is -0.15 ‰/˚C (Edwards et al., 2000). In a direct analogy, a warming of 8˚C during the PETM would

443 generate a decrease in $\delta^{13}C_p$ and an increase in discrimination of 1.2‰. Although this
444 increase is only about half of the inferred 2.5-3.2 ‰ PETM increase, discrimination in
445 Paleogene plants may been more sensitive to temperature than modern plants. The
446 PETM warming on top of an already warm climate could have caused plants to increase
447 transpiration (and thus p_i/p_a; lowering $\delta^{13}C_{TT}$ values) substantially in an effort to cool
448 their leaves during photosynthetic activity (Jones, 1992). We note that water stress is
449 expected to have a countervailing effect, and that additional studies are needed to
450 understand the sensitivity of plant physiology to the extreme climatic conditions inferred
451 for the late Paleocene and early Eocene. The conflicting influences of temperature and
452 water stress make it difficult to evaluate the influence of temperature alone in a robust
453 manner, and therefore, although intriguing, this mechanism is not considered further here.
454

455 **4.4 Hypothesis testing: Reconciling terrestrial and marine CIEs**

456 **4.4.1 Marine carbonate modification**

457 We consider two alternative hypotheses to explain the larger magnitude of the
458 CIE in the *n*-alkane record than in marine carbonates. The first is the marine modification
459 hypothesis that posits that marine carbonate records do not record the full magnitude of
460 the CIE. Significant dissolution has been identified in marine carbonates and attributed
461 to acidification of the oceans by CO_2 influx during the PETM (Zachos et al., 2005). This
462 dissolution could have removed some previously deposited carbonate and prevented the
463 deposition of carbonate during the initiation of the PETM, thereby truncating the lower
464 part of the CIE in many marine carbonate records. Such truncation would have reduced
465 the magnitude of the CIE if the largest isotopic shift occurred near the beginning.

466 However, terrestrial records, which do not suffer from dissolution, demonstrate an abrupt
467 shift in isotopic values followed by a prolonged plateau phase, rather than a strong
468 maximal excursion at the base followed by a gradual return to background (Bowen et al.,
469 2001; Dupuis et al., 2003; Magioncalda et al., 2004; Schmitz and Pujalte, 2003; Steurbaut
470 et al., 2003; Wing et al., 2005). If the CIE measured in terrestrial sequences reflects the
471 true shape of the excursion in the ocean-atmosphere carbon pool, then in order to
472 substantially decrease the apparent magnitude of the excursion in marine carbonates, the
473 entire plateau phase would have to be removed by dissolution. Such a long hiatus is not
474 supported by detailed studies of deposition in marine settings (Farley and Eltgroth, 2003;
475 Zachos et al., 2005).

476 If we rule out dissolution and non-deposition, the only remaining way to for
477 marine carbonates to fail to record the full extent of the CIE would be through direct
478 alteration of their isotope signature. We can make a quantitative estimate of the degree to
479 which the marine isotope signatures would have to be modified to bring them into
480 agreement with CIE observed in terrestrial records. Pagani et al. (2006) suggested the
481 $\delta^{13}C$ record of plant lipids might represents the true CIE in the ocean-atmosphere system
482 and that plant discrimination remained constant through the PETM. Under this scenario,
483 we can calculate the expected magnitude of the planktonic foraminifera CIE based on the
484 presumed atmospheric CO_2 excursion (drawn from the observed plant lipids $\delta^{13}C$ values)
485 and the temperature-sensitive fractionation between carbonate and atmospheric CO_2
486 (Table 3, footnote d) (Romanek et al., 1992). Given the temperature estimates for Site
487 690 (Table 3), and the lipid-based estimated CIE of 5.1‰ for atmospheric CO_2, the
488 predicted CIE for planktonic foraminifera is 6‰, reflecting both warming and the

489 changing isotopic composition of the ocean-atmosphere system. Foraminifera at Site 690
490 record a maximal CIE of 4.2‰, which is among the largest marine excursions reported
491 (Thomas et al., 2002). In order to bring the planktic foraminifera isotopic record into
492 conformity with the atmosphere under this scenario, $\delta^{13}C_{pf}$ records would have to be
493 altered such that they under-represent the true magnitude of the CIE by nearly 2‰
494 throughout the event. Declining pH might have decreased the magnitude of the excursion
495 in $\delta^{13}C_{pf}$ by ~0.5‰ (Bowen et al., 2004), but cannot explain the ~2‰ offset between the
496 predicted and observed $\delta^{13}C_{pf}$ values. No other mechanism has been identified that
497 would have reduced the preserved record of the global marine CIE by 1.5‰ or more.
498 These calculations are a conservative estimate of the degree of isotopic modification
499 required, because they use planktonic foraminifera. Benthic foraminifera generally
500 record an even smaller excursion than the planktonics (Kennett and Stott, 1991; Thomas
501 et al., 2002) and may better represent the isotopic history of the deep sea, which holds the
502 largest reservoir of carbon in the ocean-atmosphere-biosphere system.
503
504 **4.4.2 Plant community change**
505 The plant community change hypothesis invokes changes in floral composition to
506 drive a change in carbon isotope discrimination at the ecosystem level and is separate
507 from invoking an increase in discrimination by vegetation as a whole as suggested by
508 Bowen et al. (2004) and or by individual taxonomic groups as suggested by Schouten et
509 al. (2007). In the Bighorn Basin, fossil plant assemblages from the PETM demonstrate
510 almost complete turnover in the taxonomic composition of vegetation (Wing et al., 2005)
511 and *n*-alkanes show increasing Average Chain Length (ACL_{25-33}; Figure 2D & 3).

512 Similar increases in *n*-alkane ACL have been measured across the PETM in sediments
513 from the Arctic, New Zealand and the South Atlantic (Hasegawa et al., 2006; Kaiho et
514 al., 1996; Schouten et al., 2007). In modern ecosystems, ACL increases with increasing
515 temperature and precipitation, both within and among species (Sachse et al., 2006) and
516 values range widely for different taxa (Bi et al., 2005; Chikaraishi and Naraoka, 2003;
517 Collister et al., 1994; Sachse et al., 2006). Paleocene and post-PETM Eocene floras in
518 the Bighorn Basin have abundant conifers (gymnosperms), especially of the taxodiaceous
519 genera *Metasequoia* and *Glyptostrobus (*Table 2) (Wing et al., 1995). In contrast, PETM
520 floras are composed almost exclusively of angiosperms.

521 Change in floral composition could have increased the magnitude of the CIE in
522 plant lipids if, on average, immigrant species discriminated more than the species they
523 replaced. Living C_3 angiosperms generally exhibit larger discrimination than conifers,
524 both in total tissue and in *n*-alkanes (Chikaraishi and Naraoka, 2003; Flanagan et al.,
525 1997). *n*-Alkanes from C_3 angiosperms are 2.5 to 6‰ more depleted in ^{13}C than those
526 from conifers growing in the same region (Figure 5A) (Chikaraishi and Naraoka, 2003).
527 If Paleocene-Eocene conifers and angiosperms had relative discriminations similar to
528 their living relatives, the replacement of conifers by angiosperms in the Bighorn Basin
529 during the PETM should have amplified the CIE.

530 The magnitude of the shift in carbon isotope ratio resulting from the vegetational
531 change depends on the carbon isotopic composition of the components and their relative
532 biomass. Using a simple isotopic mixing model between the conifer and angiosperm
533 $\delta^{13}C$ values for each *n*-alkane, we calculate a range of potential pre-PETM isotopic
534 values for floras with different proportions of conifers. The PETM value is estimated

535 assuming a purely angiosperm flora (as indicated by the fossils) and an atmospheric
536 carbon isotope excursion of 3‰. The modeled CIE for each *n*-alkane is simply the
537 difference between isotope values for the pre-PETM (mixed community) and PETM
538 (angiosperm) flora. The pre-PETM floral compositions vary from 0-100% conifers and
539 thereby provide a large range of potential CIE curves (Figure 5B).

540 The modeled carbon isotope excursions vary significantly from one *n*-alkane to
541 the next (Figure 5B) because conifers and angiosperms differ in how their carbon isotope
542 ratios vary with chain-length. In conifers, $\delta^{13}C$ values tend to increase with increasing
543 chain length, whereas in angiosperms, they decrease (Figure 5A). Thus, the change in
544 relative abundance of conifers and angiosperms during the PETM should not only
545 amplify the CIE, but also cause the amplification to vary among *n*-alkanes of different
546 chain-lengths in a predictable way. In fact, we estimate the degree to which conifers were
547 replaced by angiosperms by comparing the measured carbon isotope excursions to the
548 modeled ones. The pattern of measured values compare very closely with the 50%
549 conifer curve (Figure 5B), suggesting that plant communities in the Bighorn Basin
550 changed from 50% conifers to an exclusively angiosperm flora at the PETM. This
551 decrease in conifer abundance is less than the raw change in leaf numbers, which go from
552 75% to 0% conifers, but is larger than the shift based on estimated leaf area, which
553 changes from 13% to 0% conifer during the PETM. Given the large number of
554 uncertainties in estimating the relative biomass of conifers from leaf fossils (e.g.,
555 potential differences in proportion of leaf to stem biomass in conifers and angiosperms,
556 potential differences in preservability), the two independent lines of evidence do not
557 appear to be inconsistent.

558

559 **4.4.3 Testable predictions of the plant community change hypothesis**

560 If reduction in conifer biomass explains the amplification of the terrestrial CIE in
561 the Bighorn Basin relative to marine records, two testable predictions can be offered. In
562 regions where conifers were rare or absent prior to the PETM, the CIE in plant lipids
563 should be of smaller magnitude. *n*-Alkanes from New Zealand may represent such
564 scenario with a stable proportion of conifers to angiosperms and a CIE of only ~3‰
565 (Kaiho et al., 1996; Crouch et al., 2003). We hypothesize that regional differences might
566 be expressed as a latitudinal gradient, with tropical and subtropical regions having
567 angiosperm-dominated vegetation during the Paleocene and demonstrating smaller CIEs
568 than mid and high latitude regions where conifers were abundant to dominant. A
569 latitudinal gradient is suggested by *n*-alkanes from the Arctic (Pagani et al., 2006) that
570 record a CIE that is ~1 ‰ larger than in the Bighorn Basin. Pollen from the Arctic Ocean
571 records a large increase in angiosperms (from 40% to 72% during the PETM), at the
572 expense of gymnosperms (from 33% to 18% during the PETM) (Sluijs et al., 2006).

573 A second prediction of the plant community change hypothesis is that the
574 amplification of carbon isotope excursions should vary among the different chain-lengths
575 of *n*-alkanes in a predictable pattern depending on the degree to which angiosperms
576 displaced conifers. If the degree of displacement increased with latitude, the predicted
577 pattern would be like that in Figure 5B, with low latitude sites corresponding to the lower
578 proportion and high latitude sites to higher proportion of conifers in the pre-PETM flora.
579 Therefore, both the magnitude and curvature of the CIE-chain length relationship should
580 vary regionally, and in general increase with increasing latitude.

581

582 **5. CONCLUSIONS**

583 High-molecular weight *n*-alkanes derived from vascular plant leaf waxes are well
584 preserved across the PETM interval in the Cabin Fork area of the Bighorn Basin. The
585 carbon-isotope record of *n*-alkanes shows a large negative carbon isotope excursion of ~
586 4-5‰. This CIE is 1-2‰ larger than that observed in the bulk organic matter from the
587 same samples and elsewhere, and that observed in marine carbonates. The carbon isotope
588 record of leaf lipids demonstrates that bulk soil organic matter records do not capture the
589 full magnitude of the carbon isotope excursion in plants at the PETM.

590 We use the *n*-alkane and marine carbonate isotopic records to estimate carbon-
591 isotope discrimination by plants across the PETM, and infer that for this locality plant
592 discrimination increased by 2.5-3.2‰. Changes in plant discrimination in the historic
593 and geologic past are frequently related to changes in available moisture, because this is a
594 key control on discrimination in modern ecosystems. However, three lines of evidence,
595 hydrogen isotope ratios of *n*-alkanes, paleosol properties, and leaf physiognomy, are not
596 consistent with an increase in relative humidity during the PETM. Instead, they suggest
597 cycles of wet and dry conditions.

598 Modification of marine carbonate records such that they fail to record the full
599 magnitude of the CIE would create the impression of enhanced terrestrial plant
600 discrimination. However, if we assume that the plant lipids directly reflect atmospheric
601 CO_2 $\delta^{13}C$ values, and we take the warming into consideration, the expected planktonic
602 foram CIE (6‰) is much larger than the maximum observed marine excursion of 4.2‰.
603 There is no known mechanism that could modify the marine record enough to account for

604 this difference and we conclude instead that carbon isotope discrimination in plants
605 increased during the PETM.

606 We propose that observed changes in floral assemblages from a mixed
607 angiosperm/conifer to an exclusively angiosperm flora at the PETM increased ecosystem
608 carbon isotope discrimination in the Bighorn Basin. Because angiosperms discriminate
609 more than conifers, the floral change amplified the carbon isotope excursion relative to
610 the ocean-atmosphere reservoir. The degree of amplification is modeled and compared to
611 measured values for each *n*-alkane chain length. The modeled values capture not only
612 the magnitude of the observed CIE amplification but also the pattern of amplification
613 among the different chain-length *n*-alkanes. In addition, the data-model comparison
614 suggests that the PETM caused a shift from floras that were 50% conifers and 50%
615 angiosperms to floras that were 100% angiosperms.

616 The balance of evidence strongly supports the plant community change
617 hypothesis for reconciling the terrestrial and marine carbon isotope excursions at the
618 PETM and suggests two testable predictions. The magnitude of the CIE in leaf-wax *n*-
619 alkanes should vary regionally, depending on the extent of plant community change. If
620 angiosperms expanded poleward, replacing conifers, the magnitude of the carbon isotope
621 excursion in plant lipids would increase with increasing latitude. A preliminary
622 suggestion of such a gradient is evident in the leaf-wax CIE in the Arctic being ~1‰
623 larger than in the Bighorn Basin. The second prediction is that the pattern of
624 amplification of the CIE among the *n*-alkanes should also vary regionally, perhaps even
625 latitudinally, in a predictable fashion reflecting shifts in relative abundance of conifers

626 and angiosperms. Tests of these predictions will require additional latitudinal sampling
627 of leaf waxes from the PETM.
628
629 **ACKNOWLEDGEMENTS**
630 We would like to thank Dennis Walizer, Christopher Lernihan and Pratigya Polissar for
631 laboratory assistance, Amy Morey for counting fossil leaves, David Beausang for field
632 assistance, Douglas Boyer for DGPS work and stratigraphic model, and Jon Bloch for
633 real-time biostratigraphy. We also would like to thank Aradhna Tripati and Deborah
634 Thomas for providing raw data for foram isotope ratios. This manuscript greatly
635 benefited from the comments of three anonymous reviewers.

Table 1: *n*-Alkane $\delta^{13}C$, δD, and Average chain length.

		$\delta^{13}C_{n\text{-alkane}}$										$\delta D_{n\text{-alkane}}$		ACL
Meter level	Sample	C25 Avg.	C25 S.D.	C27 Avg.	C27 S.D.	C29 Avg.	C29 S.D.	C31 Avg.	C31 S.D.	C33 Avg.	C33 S.D.	C29 Avg.	C29 s.d.	C25 to C33
-19.95	CAB3-04-06	-29.1	0.4	-29.5	0.0	-30.9	0.1	-31.6	0.0			-186	1.4	28.6
-13.75	CAB3-04-07	-29.7	0.1	-30.3	0.1	-31.1	0.1	-31.4	0.0			-196	0.9	28.7
-0.85	CAB7-04-02	-33.7	0.2	-34.0	0.0	-35.5	0.0	-36.5	0.0	-37.4	0.1	-183	1.3	30.1
-0.15	CAB7-04-03	-33.5	0.5	-33.0	0.1	-34.1	0.1	-35.8	0.0	-36.0	0.0			29.0
8.20	CAB1-04-06			-34.8	0.3	-35.3	0.1	-36.3	0.0	-36.9	0.2	-190		30.6
37.30	CAB6-04-01.1			-33.0	0.2	-33.2	0.3	-34.5	0.2	-35.7		-197	1.0	29.4
45.30	SW0306	-29.3	0.8	-30.0	0.3	-30.6	0.1	-32.0	0.3	-31.3	0.0	-192	0.3	28.7
73.30	CAB6-04-04	-29.6	0.3	-29.9	0.0	-30.8	0.0	-31.8	0.2	-31.6		-196	0.9	28.9

Table 2: Abundance of fossil leaves of major plant groups

	Conifer		Dicot		Monocot		Ginkgo		Pteridophyte	
	N	%	N	%	N	%	N	%	N	%
earliest Eocene (post-PETM)	4794	0.75	1477	0.23	49	0.01	42	0.01	3	0.00
PETM	0	0.00	1985	0.99	8	0.00	0	0.00	2	0.00
latest Paleocene	16506	0.76	5043	0.23	92	0.00	95	0.00	57	0.00

Table 3: Planktonic foraminifera data used to estimate $\delta^{13}C$ of atmospheric CO_2

ODP Site 690 (Thomas et al., 2002) (Thomas et al., 2002)

	Depth interval (mbsf)	$\delta^{13}C_{pf}$ (‰ VPDB) *Acaranina* sp.	Std. Dev. (n)	$\delta^{18}O_{pf}$ (‰ VPDB) *Acaranina* sp.	Std. Dev. (n)	Temperature from $\delta^{18}O$ (˚C)[a]	$\alpha_{CO2\text{-}Calcite}$[d]	$\delta^{13}C_{Atm}$ (‰ VPDB)
Pre-CIE	171.02-170.79	3.37	0.33 (36)	-0.20	0.25 (36)	13.4	0.9897	-6.9
Peak CIE	170.77-170.60	-0.20	0.69 (88)	-1.51	0.18 (88)	19.5	0.9905	-9.7
Recovery	170.26-169.84	1.55	0.43 (44)	-2.35	0.27 (44)	23.2	0.9909	-7.6

ODP Site 1209 (Zachos et al., 2003) (Zachos et al., 2003).

	Depth interval (m in section 1209B-22H-1)	$\delta^{13}C_{pf}$ (‰ VPDB) A. soldadoensis	Std. Dev. (n)	$\delta^{18}O_{pf}$ (‰ VPDB) A. soldadoensis	Std. Dev. (n)	Temperature from $\delta^{18}O$ (˚C)[b]	$\alpha_{CO2\text{-}Calcite}$[d]	$\delta^{13}C_{Atm}$ (‰ VPDB)
Pre-CIE	1.48-1.39	3.86	0.28 (11)	-1.42	0.17 (11)	22.5	0.9908	-5.4
Peak CIE	1.34-1.30	1.14	0.59 (19)	-1.70	0.20 (19)	26.6	0.9913	-7.6
Recovery	1.14-1.09	2.01	0.24 (6)	-1.23	0.16 (6)	24.5	0.9910	-7.0
Post-CIE	0.94-0.89	3.14	0.27 (4)	-1.36	0.20 (4)	22.3	0.9908	-6.1

ODP Site 1209 (Zachos et al., 2003) (Zachos et al., 2003).

	Depth interval (m in section 1209B-22H-1)	$\delta^{13}C_{pf}$ (‰ VPDB) A. soldadoensis	Std. Dev. (n)	Mg/Ca A. soldadoensis	Std. Dev. (n)	Temperature from Mg/Ca (˚C)[c]	$\alpha_{CO2\text{-}Calcite}$[d]	$\delta^{13}C_{Atm}$ (‰ VPDB)
Pre-CIE	1.48-1.39	3.86	0.28 (11)	3.68	0.06 (3)	30.6	0.9918	-4.4
Peak CIE	1.34-1.30	1.14	0.59 (19)	5.05	0.19 (5)	33.6	0.9921	-6.7
Recovery	1.14-1.09	2.01	0.24 (6)	4.48	0.34 (2)	32.7	0.9920	-6.0
Post-CIE	0.94-0.89	3.14	0.27 (4)	3.81	0.06 (3)	30.9	0.9918	-5.1

[a] Calculated using T (˚C) = 16.998 + -4.52 $(\delta^{18}O_{pf} - \delta^{18}O_{sw})$ + 0.028 $(\delta^{18}O_{pf} - \delta^{18}O_{sw})^2$ (Erez and Luz, 1983) and $\delta^{18}Osw$ = -1 ‰ for an ice-free world.
[b] Calculated using equation in [a] (Erez and Luz, 1983) with $\delta^{18}Osw$ = -0.2 ‰ before and after PETM and $\delta^{18}Osw$ = 0.4 ‰ during the PETM and recovery based on inferred change in Salinity at site 1209 across the PETM (Zachos et al., 2003).

[c] Calculated using Mg/Ca = 0.38*f* exp(0.09T) using seawater Mg/Ca fraction relative to modern (*f*) of 0.62 (Tripati and Elderfield, 2004).

[d] Fractionation factor calculated as $\alpha_{CO2\text{-}Calcite} = R_{CO2}/R_{Calcite} = 1/[1.01198 - 0.00012\ T(^{\circ}C)]$ (Romanek et al., 1992).

Table 4: Carbon isotope discrimination (Δ) and Pi/Pa ratios calculated from $\delta^{13}C_{TT}$ and three estimates of $\delta^{13}C_{Atm}$ (Table 3).

				$\delta^{13}C_{Atm}$ from 690		$\delta^{13}C_{Atm}$ from 1209 ($\delta^{18}O$)		$\delta^{13}C_{Atm}$ from 1209 (Mg/Ca)	
Meter	Interval	Sample #	$\delta^{13}C_{TT}$[a]	Δ	Pi/Pa	Δ	Pi/Pa	Δ	Pi/Pa
-19.95	Pre-CIE	CAB3-04-06	-26.8			22.1	0.78	23.0	0.82
-13.75	Pre-CIE	CAB3-04-07	-26.6	20.2	0.70	21.8	0.77	22.8	0.81
-0.85	Peak CIE	CAB7-04-02	-31.7	22.7	0.81	25.0	0.91	25.8	0.95
-0.15	Peak CIE	CAB7-04-03	-31.1	22.0	0.78	24.3	0.88	25.1	0.92
8.2	Peak CIE	CAB1-04-06	-31.6	22.5	0.80	24.8	0.90	25.6	0.94
37.3	Recovery	CAB6-04-01.1	-29.7	22.8	0.82	23.5	0.84	24.5	0.89
45.3	Post-CIE	SW0306	-27.2			21.7	0.76	22.7	0.81
73.3	Post-CIE	CAB6-04-04	-27.1			21.5	0.76	22.6	0.80

[a] $\delta^{13}C_{TT}$ calculated from C_{31} *n*-alkane using ε = 4.9‰ from compilation of published data (Bi et al., 2005; Chikaraishi and Naraoka, 2003; Collister et al., 1994).

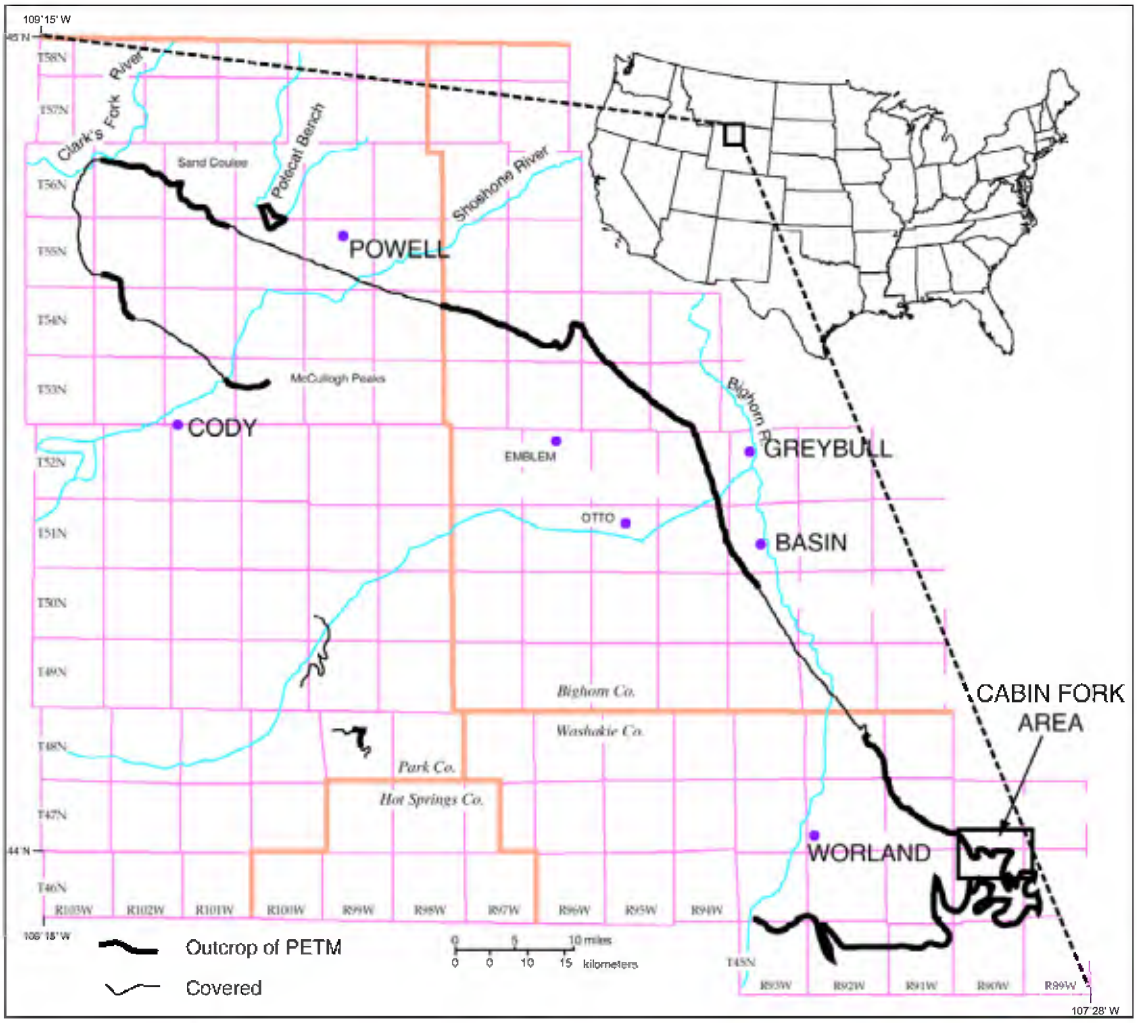

Figure 1. Map of study area on Cabin Fork of Nowater Creek. Black line indicates Paleocene-Eocene contact, and is thick where exposed and thin where covered.

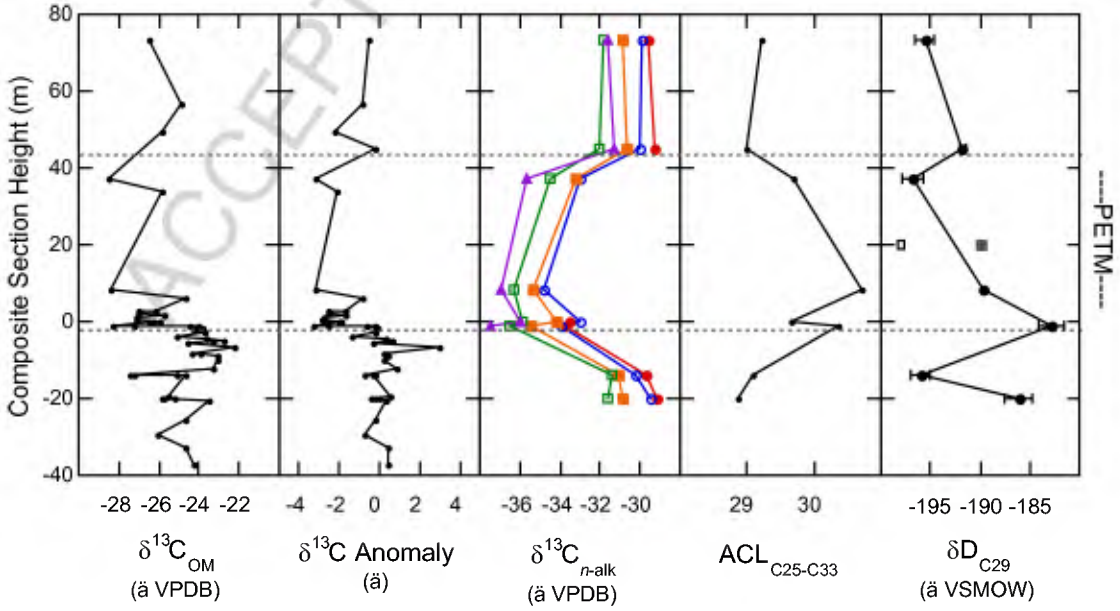

Figure 2

Carbon isotope, hydrogen isotope and average chain length (ACL) records from the composite section from the Cabin Fork area of the Bighorn basin. A) Bulk $\delta^{13}C$ for organic matter. B) Difference between measured value (A) and the value predicted based on the weight % organic carbon for each sample using logarithmic relationship for background conditions (Wing et al., 2005). C) Compound-specific $\delta^{13}C$ for C_{25} to C_{33} *n*-alkanes. C_{25}: solid red circles, C_{27}: open blue circles, C_{29}: solid orange squares, C_{31}: open green squares, C_{33}: solid purple triangles. Measurement precision for all $\delta^{13}C$ values is less than the represented by the data symbols. D) Average chain length calculated as the abundance-weighted average of the odd *n*-alkanes from C_{25} through C_{33}. E) Compound-specific δD for C_{29}: solid circles. Error bars for δD represent ± 1 standard deviation of replicate measurements. Predicted PETM δD_{C29} values (squares) based on leaf water model and δD of surface waters estimated from $\delta^{18}O$ of tooth enamel; with constant RH of 60%: grey square; with a 25% increased in RH during the PETM: open square.

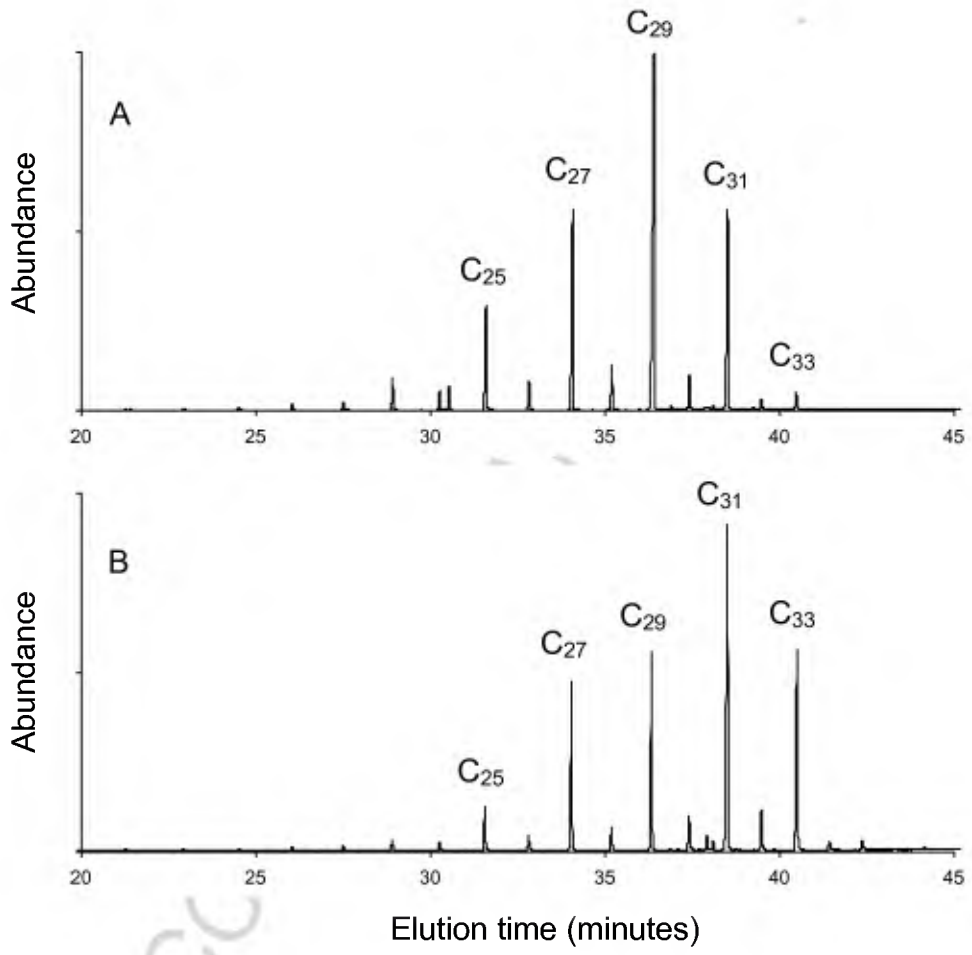

Figure 3

Total ion chromatogram for the non-polar lipid fraction from sediments from (A) immediately before the PETM (-13.75 m; Cab3-04-07) and (B) at the base of the PETM (-0.85 m; Cab7-04-02). Labeled high molecular weight odd-carbon numbered *n*-alkanes are those used to calculate average chain length (Figure 2D, Table 1).

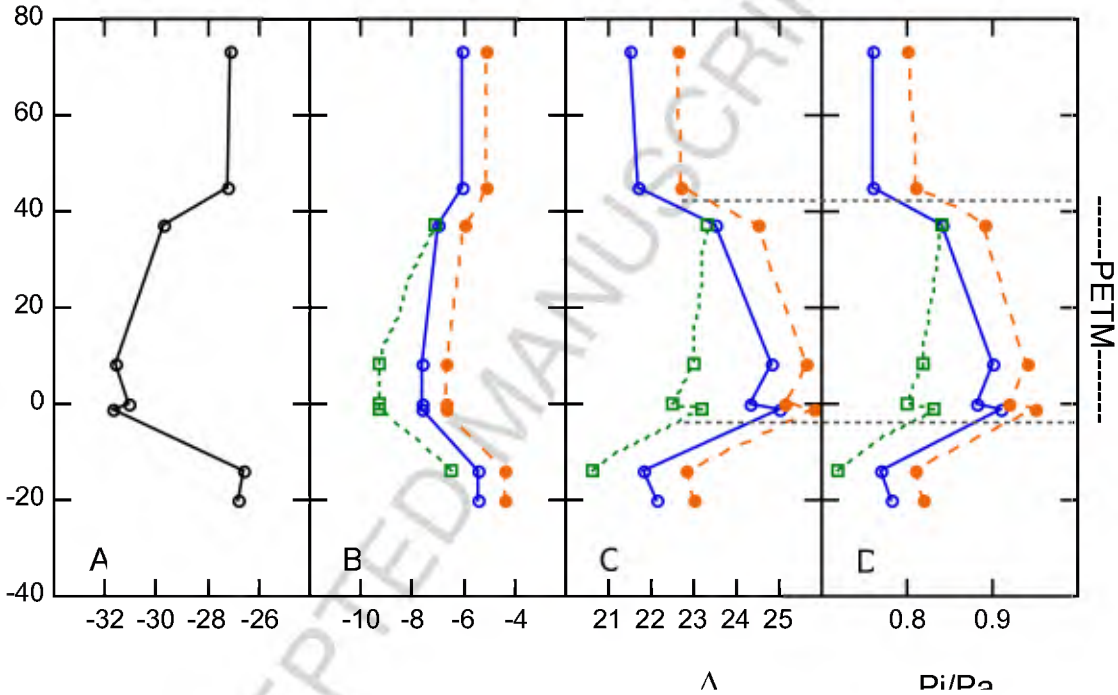

Figure 4
Carbon isotope ratios (‰ VPDB) of A) plant total tissue calculated from C_{31} *n*-alkane and B) atmospheric CO_2 calculated from carbon isotope ratios of planktonic forams from ODP sites 1209 and 690 (Table 3). Open green squares and dotted line- Site 690 using $\delta^{18}O$ temperature estimates. Open blue circles and solid line- Site 1209 using $\delta^{18}O$ temperature estimates. Orange filled circles- Site 1209 using Mg/Ca temperature estimates. C) ^{13}C-discrimination by plants (Δ) relative to atmospheric CO_2. D) Partial pressure of CO_2 inside the leaf (p_i) relative to that in the atmosphere (p_a). Colors and symbols in C and D correspond to those in B.

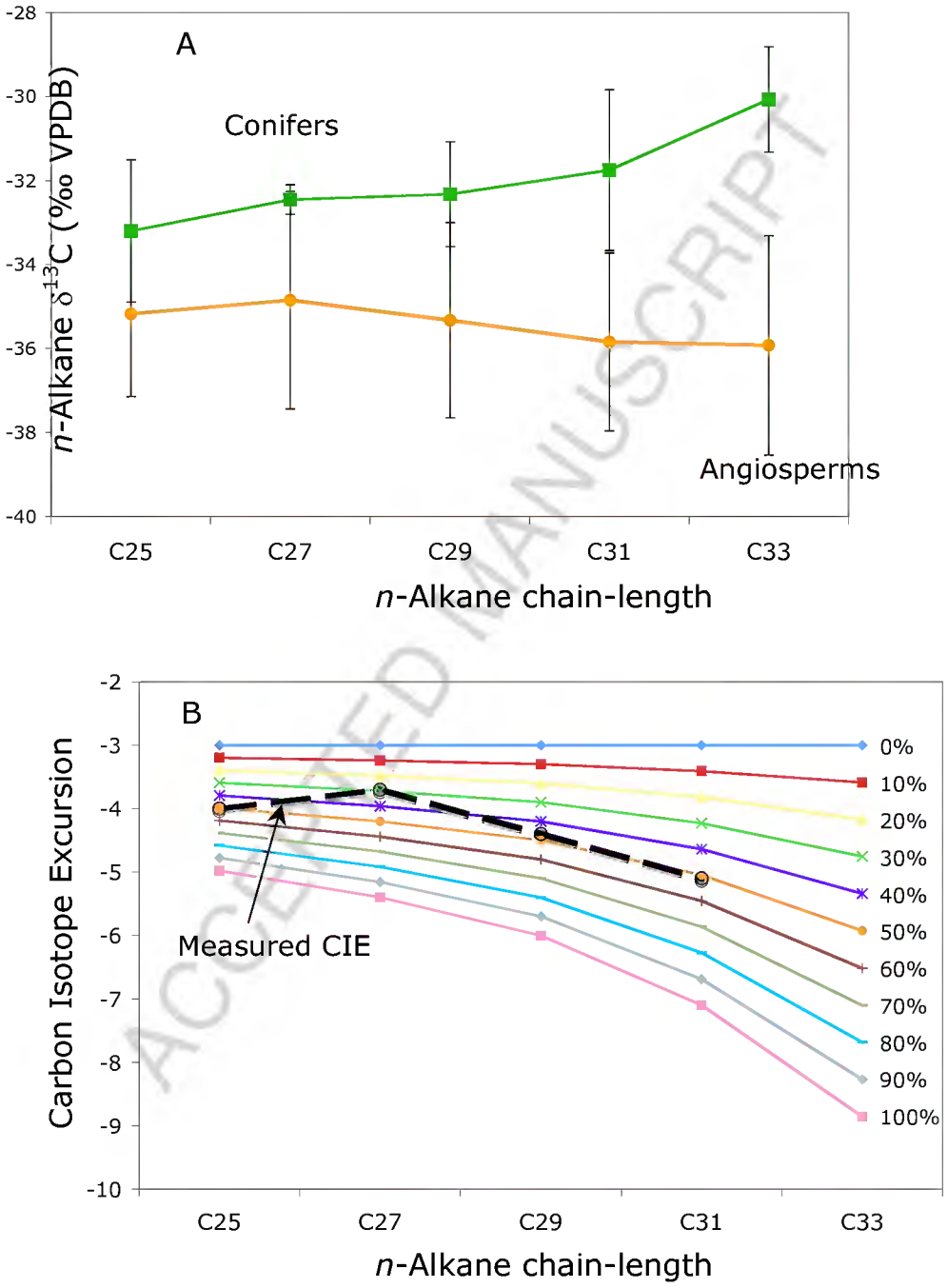

Figure 5
(A) *n*-Alkane $\delta^{13}C$ values of modern conifers and C_3 dicotyledonous angiosperms (compilation of data from Bi et al., 2005; Chikaraishi and Naraoka, 2003; Collister et al., 1994). Error bars are 1 S.D. Conifer: N = 2 to 4. Angiosperm: N = 30 to 42. (B) Predicted CIEs based on a shift from pre-PETM floras of varying proportions of conifers (percentages on figure) to PETM floras that are exclusively angiosperms. The taxonomic effect is added to a baseline CIE of -3‰. Solid lines indicate varying pre-PETM conifer percentages (0-100%). Open circles and dashed line indicates measured CIE values.

BIBLIOGRAPHY

Arens, N.C., Jahren, A.H., Amundson, R., 2000. Can C_3 plants faithfully record the carbon isotopic composition of atmospheric carbon dioxide? Paleobiology, 26: 137-164.

Bains, S., Corfield, R.M., Norris, R.D., 1999. Mechanisms of climate warming at the end of the Paleocene. Science, 285: 724-727.

Beard, K.C., Dawson, M.R., 1999. Intercontinental dispersal of Holarctic land mammals near the Paleocene/Eocene boundary: paleogeographic, paleoclimatic and biostratigraphic implications. Bulletin De La Societe Geologique De France, 170: 697-706.

Beerling, D.J., 1996. Ecophysiological responses of woody plants to past CO_2 concentrations. Tree Physiology, 16: 389-396.

Beerling, D.J., Woodward, F.I., 1995. Leaf stable carbon-isotope composition records increased water-use efficiency of C_3 plants in response to atmospheric CO_2 enrichment. Functional Ecology, 9: 394-401.

Bi, X., Sheng, G., Liu, X., Li, C., Fu, J., 2005. Molecular and carbon and hydrogen isotopic composition of *n*-alkanes in plant leaf waxes. Organic Geochemistry, 36: 1405-1417.

Bloch, J.I., Boyer , D.M., Strait, S.G., Wing, S.L., 2004. New sections and fossils from the southern Bighorn Basin, Wyoming document faunal turnover during the PETM. Eos Trans. AGU, 85.

Bolle, M.P., Adatte, T., 2001. Palaeocene early Eocene climatic evolution in the Tethyan realm: clay mineral evidence. Clay Minerals, 36: 249-261.

Bowen, G.J., Beerling, D.J., Koch, P.L., Zachos, J.C., Quattlebaum, T., 2004. A humid climate state during the Palaeocene/Eocene thermal maximum. Nature, 432: 495-499.

Bowen, G.J., Koch, P.L., Gingerich, P.D., Norris, R.D., Bains, S., Corfield, R.M., 2001. Refined isotope stratigraphy across the continental Paleocene-Eocene boundary on polecat bench in the northern Bighorn Basin. In: P.D. Gingerich (Editor), Paleocene-Eocene Stratigraphy and Biotic Change in the Bighorn and Clarks Fork Basins, Wyoming. University of Michigan Papers on Paleontology 33. Museum of Paleontology, The University of Michigan, Ann Arbor, MI, pp. 73-88.

Bowling, D.R., McDowell, N.G., Bond, B.J., Law, B.E., Ehleringer, J.R., 2002. C-13 content of ecosystem respiration is linked to precipitation and vapor pressure deficit. Oecologia, 131: 113-124.

Bown, T.M., 1980. Summary of latest Creataceous and Cenozoic sedimentary, tectonic and erosional events, Bighorn Basin, Wyoming. In: P.D. Gingerich (Editor), Early Cenozoic Paleontology and Stratigraphy of the Bighorn Basin, Wyoming. University of Michicagn Papers on Paleontology. Univeristy of Michigan, Ann Arbor, MI, pp. 5-32.

Burgoyne, T.W., Hayes, J.M., 1998. Quantitative production of H_2 by pyrolysis of gas chomatographic effluents. Analytical Chemistry, 70: 5136-5141.

Burnham, R.J., Wing, S.L., Parker, G.G., 1992. The reflection of deciduous forest communities in leaf litter: implications for autochthonous litter assemblages from the fossil record. Paleobiology, 18: 30-49.

Cerling, T.E., 1984. The stable isotopic composition of modern soil carbonate and its relationship to climate. Earth and Planetary Science Letters, 71: 229-240.

Chikaraishi, Y., Naraoka, H., 2003. Compound-specific δD-δ^{13}C analyses of *n*-alkanes extracted from terrestrial and aquatic plants. Phytochemistry, 63: 361-371.

Clyde, W.C., Gingerich, P.D., 1998. Mammalian community response to the latest Paleocene thermal maximum: An isotaphonomic study in the northern Bighorn Basin, Wyoming. Geology, 26: 1011-1014.

Collister, J.W., Rieley, G., Stern, B., Eglinton, G., Fry, B., 1994. Compound-specific δ^{13}C analyses of leaf lipids from plants with differing photosynthetic pathways. Organic Geochemistry, 21: 619-627.

Craig, H., 1961. Isotope variations in meteoric water. Science, 133: 1702-1703.

Craig, H., Gordon, L.I., 1965. Deuterium and oxygen-18 variations in the ocean and the marine atmosphere. In: E. Tongiorgi (Editor), Proceedings of the Third Spoletto Conference on Stable Isotopes in Oceanographic Studies and Paleotemperatures. CNR-Laboratorio di Geologia Nucleare, pp. 9-130.

Cramer, B.S., Aubry, M.P., Miller, K.G., Olsson, R.K., Wright, J.D., Kent, D.V., 1999. An exceptional chronologic, isotopic, and clay mineralogic record of the latest Paleocene thermal maximum, Bass River, NJ, ODP 144AX. Bulletin De La Societe Geologique De France, 170: 883-897.

Crouch, E.M., Dickens, G.R., Brinkhuis, H., Aubry, M.P., Hollis, C.J., Rogers, K.M., Visscher, H., 2003. The Apectodinium acme and terrestrial discharge during the Paleocene-Eocene thermal maximum: new palynological, geochemical and calcareous nannoplankton observations at Tawanui, New Zealand. Palaeogeography Palaeoclimatology Palaeoecology, 194: 387-403.

Crouch, E.M., Heilmann-Clausen, C., Brinkhuis, H., Morgans, H.E.G., Rogers, K.M., Egger, H., Schmitz, B., 2001. Global dinoflagellate event associated with the late Paleocene thermal maximum. Geology, 29: 315-318.

Dickens, G.R., O'Neil, J.R., Rea, D.K., Owen, R.M., 1995. Dissociation of oceanic methane hydrate as a cause of the carbon isotope excursion at the end of the Paleocene. Paleoceanography, 10: 965-971.

Dupuis, C., Aubry, M.P., Steurbaut, E., Berggren, W.A., Ouda, K., Magioncalda, R., Cramer, B.S., Kent, D.V., Speijer, R.P., Heilmann-Clausen, C., 2003. The Dababiya Quarry section: Lithostratigraphy, clay mineralogy, geochemistry and paleontology. Micropaleontology, 49: 41-59.

Edwards, T.W.D., Graf, W., Trimborn, P., Stichler, W., Lipp, J., Payer, H.D., 2000. δ^{13}C response surface resolves humidity and temperature signals in trees. Geochimica et Cosmochimica Acta, 64: 161-167.

Eglinton, G., Hamilton, R.J., 1967. Leaf epicuticular waxes. Science, 156: 1322-1334.

Erez, J., Luz, B., 1983. Experimental paleotemperature equation for planktonic foraminifera. Geochimica et Cosmochimica Acta, 47: 1025-1031.

Farley, K.A., Eltgroth, S.F., 2003. An alternative age model for the Paleocene-Eocene thermal maximum using extraterrestrial He-3. Earth and Planetary Science Letters, 208: 135-148.

Farquhar, G.D., Ehleringer, J.R., Hubick, K.T., 1989. Carbon isotope discrimination and photosynthesis. Annual Review of Plant Physiology and Plant Molecular Biology, 40: 503-537.

Flanagan, L.B., Brooks, J.R., Ehleringer, J.R., 1997. Photosynthesis and carbon isotope discrimination in boreal forest ecosystems: A comparison of functional characteristics in plants from three mature forest types. Journal of Geophysical Research-Atmospheres, 102: 28861-28869.

Freeman, K.H., Colarusso, L.A., 2001. Molecular and isotopic records of C_4 grassland expansion in the late Miocene. Geochimica et Cosmochimica Acta, 65: 1439-1454.

Freeman, K.H., Pagani, M., 2005. Alkenone-based estimates of past CO_2 levels: A consideration of their utility based on an analysis of uncertainties. In: J.R. Ehleringer, T.E. Cerling, M.D. Dearing (Editors), A History of Atmospheric CO2 and Its Effects on Plants, Animals, and Ecosystems. Springer, New York, pp. 35-61.

Fricke, H.C., Clyde, W.C., O'Neil, J.R., Gingerich, P.D., 1998. Evidence for rapid climate change in North America during the latest Paleocene thermal maximum: Oxygen isotope composition of biogenic phosphate from the Bighorn Basin (Wyoming). Earth and Planetary Science Letters, 160: 193-208.

Fricke, H.C., Wing, S.L., 2004. Oxygen isotope and paleobotanical estimates of temperature and $\delta^{18}O$-latitude gradients over North America during the early Eocene. American Journal of Science, 304: 612-635.

Gibbs, S.J., Bown, P.R., Sessa, J.A., Bralower, T.J., Wilson, P.A., 2006. Nannoplankton Extinction and Origination Across the Paleocene-Eocene Thermal Maximum. Science, 314: 1770-1773.

Gibson, T.G., Bybell, L.M., Mason, D.B., 2000. Stratigraphic and climatic implications of clay mineral changes around the Paleocene/Eocene boundary of the northeastern US margin. Sedimentary Geology, 134: 65-92.

Gingerich, P.D., 2001. Biostratigraphy of the continental Paleocene-Eocene boundary interval on Polecat Bench in the northern Bighorn Basin. In: P.D. Gingerich (Editor), Paleocene-Eocene Stratigraphy and Biotic Change in the Bighorn and Clarks Fork Basins, Wyoming. Museum of Paleontology, The University of Michigan, Ann Arbor, MI, pp. 37-71.

Gingerich, P.D., 2003. Mammalian responses to climate change at the Paleocene-Eocene boundary: Polecat Bench record in the northern Bighorn Basin, Wyoming. In: S.L. Wing, P.D. Gingerich, B. Schmitz, E. Thomas (Editors), Causes and Consequences of Globally Warm Climates in the Early Paleogene. Geological Society of America Special Paper. Geological Society of America, Boulder, CO.

Hasegawa, T., Yamamoto, S., Pratt, L.M., 2006. Data report: stable carbon isotope fluctuation of long-chain n-alkanes from Leg 208 Hole 1263A across the Paloecene/Eocene boundary. In: D. Kroon, J.C. Zachos, C. Richter (Editors), Proc. ODP, Sci. Results, vol. 208. Ocean Drilling Program, College Sation Texas, pp. doi:10.2973/odp.proc.sr.208.202.2006.

Higgins, J.A., Schrag, D.P., 2006. Beyond methane: Towards a theory for the Paleocene-Eocene Thermal Maximum. Earth and Planetary Science Letters, 245: 523-537.

Hilkert, A.W., Douthitt, C.B., Schlüter, H.J., Brand, W.A., 1999. Isotope ratio monitoring gas chromatography/mass spectrometry of D/H by high temperature conversion isotope ratio mass spectrometry. Rapid Communications in Mass Spectrometry, 13: 1226-1230.

Huber, M., Sloan, L.C., 1999. Warm climate transitions: A general circulation modeling study of the Late Paleocene thermal maximum (about 56 Ma). Journal of Geophysical Research-Atmospheres, 104: 16633-16655.

Jones, H.G., 1992. Plants and Microclimate. Cambridge University Press, Cambridge.

Kaiho, K., Arinobu, T., Ishiwatari, R., Morgans, H.E.G., Okada, H., Takeda, N., Tazaki, K., Zhou, G., Kajiwara, Y., Matsumoto, R., Hirai, A., Niitsuma, N., Wada, H., 1996. Latest Paleocene benthic foraminiferal extinction and environmental changes at Tawanui, New Zealand. Paleoceanography, 11: 447-465.

Kelly, D.C., 2002. Response of Antarctic (ODP Site 690) planktonic foraminifera to the Paleocene-Eocene thermal maximum: Faunal evidence for ocean/climate change. Paleoceanography, 17.

Kennett, J.P., Stott, L.D., 1991. Abrupt Deep-Sea Warming, Palaeoceanographic Changes and Benthic Extinctions at the End of the Paleocene. Nature, 353: 225-229.

Kent, D.V., Cramer, B.S., Lanci, L., Wang, D., Wright, J.D., Van der Voo, R., 2003. A case for a comet impact trigger for the Paleocene/Eocene thermal maximum and carbon isotope excursion. Earth and Planetary Science Letters, 211: 13-26.

Koch, P.L., Zachos, J.C., Dettman, D.L., 1995. Stable-Isotope Stratigraphy and Paleoclimatology of the Paleogene Bighorn Basin (Wyoming, USA). Palaeogeography Palaeoclimatology Palaeoecology, 115: 61-89.

Koch, P.L., Zachos, J.C., Gingerich, P.D., 1992. Correlation between Isotope Records in Marine and Continental Carbon Reservoirs near the Paleocene Eocene Boundary. Nature, 358: 319-322.

Kraus, M.J., Riggins, S., 2007. Transient drying during the Paleocene-Eocene Thermal Maximum (PETM): Analysis of paleosols in the bighorn basin, Wyoming. Palaeogeography, Palaeoclimatology, Palaeoecology, 245: 444-461.

Kurtz, A.C., Kump, L.R., Arthur, M.A., Zachos, J.C., Paytan, A., 2003. Early Cenozoic decoupling of the global carbon and sulfur cycles. Paleoceanography, 18.

Magioncalda, R., Dupuis, C., Smith, T., Steurbaut, E., Gingerich, P.D., 2004. Paleocene-Eocene carbon isotope excursion in organic carbon and pedogenic carbonate: Direct comparison in a continental stratigraphic section. Geology, 32: 553-556.

Metz, B., Davidson, O., Swart, R., Pan, J. (Editors), 2001. Contribution of Working Group III to the Third Assessment Report of the Intergovernmental Panel on Climate Change (IPCC). Cambridge University Press., Cambridge, England, 700 pp.

Pagani, M., Pedentchouk, N., Huber, M., Sluijs, A., Schouten, S., Brinkhuis, H., Sinninghe Damste, J.S., Dickens, G.R., Expedition, S., 2006. Arctic hydrology during global warming at the Palaeocene/Eocene thermal maximum. Nature, 442: 671-675.

Polley, H.W., Johnson, H.B., Marino, B.D., Mayeux, H.S., 1993. Increase in C_3 plant water-use efficiency and biomass over glacial to present CO_2 concentrations. Nature, 361: 61-64.

Robert, C., Kennett, J.P., 1994. Antarctic Subtropical Humid Episode at the Paleocene-Eocene Boundary - Clay-Mineral Evidence. Geology, 22: 211-214.

Roden, J.S., Ehleringer, J.R., 1999. Observations of hydrogen and oxygen isotopes in leaf water confirm the Craig-Gordon model under wide-ranging environmental conditions. Plant Physiology, 120: 1165-1173.

Rohl, U., Bralower, T.J., Norris, R.D., Wefer, G., 2000. New chronology for the late Paleocene thermal maximum and its environmental implications. Geology, 28: 927-930.

Romanek, C.S., Grossman, E.L., Morse, J.W., 1992. Carbon Isotopic Fractionation in Synthetic Aragonite and Calcite - Effects of Temperature and Precipitation Rate. Geochimica et Cosmochimica Acta, 56: 419-430.

Sachse, D., Radke, J., Gleixner, G., 2006. δD values of individual *n*-alkanes from terrestrial plants along a climatic gradient - Implications for the sedimentary biomarker record. Organic Geochemistry, 37: 469-483.

Saurer, M., Siegwolf, R.T.W., Schweingruber, F.H., 2004. Carbon isotope discrimination indicates improving water-use efficiency of trees in northern Eurasia over the last 100 years. Global Change Biology, 10: 2109-2120.

Schmitz, B., Pujalte, V., 2003. Sea-level, humidity, and land-erosion records across the initial Eocene thermal maximum from a continental-marine transect in northern Spain. Geology, 31: 689-692.

Schouten, S., Woltering, M., Rijpstra, W.I.C., Sluijs, A., Brinkhuis, H., Sinninghe Damste, J.S., 2007. The Paleocene-Eocene carbon isotope excursion in higher plant organic matter: Differential fractionation of angiosperms and conifers in the Arctic. Earth and Planetary Science Letters, 258: 581-592.

Sessions, A.L., Burgoyne, T.W., Hayes, J.M., 2001. Determination of the H_3 factor in hydrogen isotope ratio monitoring mass spectrometry. Analytical Chemistry, 73: 200-207.

Shellito, C.J., Sloan, L.C., Huber, M., 2003. Climate model sensitivity to atmospheric CO2 levels in the Early-Middle Paleogene. Palaeogeography, Palaeoclimatology, Palaeoecology, 193: 113-123.

Sluijs, A., Schouten, S., Pagani, M., Woltering, M., Brinkhuis, H., Damsté, J.S.S., Dickens, G.R., Huber, M., Reichart, G.-J., Stein, R., Matthiessen, J., Lourens, L.J., Pedentchouk, N., Backman, J., Moran, K., the Expedition, S., 2006. Subtropical Arctic Ocean temperatures during the Palaeocene/Eocene thermal maximum. Nature, 441: 610-613.

Smith, F.A., Freeman, K.H., 2006. Influence of physiology and climate on δD of leaf wax *n*-alkanes from C_3 and C_4 grasses. Geochimica et Cosmochimica Acta, 70: 1172-1187.

Steurbaut, E., Magioncalda, R., Dugas, D.P., Van Simaeys, S., Roche, E., Roche, M., 2003. Palynology, paleoenvironments and organic carbon isotope evolution in lagoonal Paleocene-Eocene boundary settings in northern Belgium. In: S.L. Wing, P.D. Gingerich, B. Schmitz, E. Thomas (Editors), Causes and Consequences of Globally Warm Climates in the Early Paleogene. Geological Society of America, Boulder, CO, pp. 291-317.

Svensen, H., Planke, S., Malthe-Sorenssen, A., Jamtveit, B., Myklebust, R., Eidem, T.R., Rey, S.S., 2004. Release of methane from a volcanic basin as a mechanism for initial Eocene global warming. Nature, 429: 542-545.

Thomas, D.J., Zachos, J.C., Bralower, T.J., Thomas, E., Bohaty, S., 2002. Warming the fuel for the fire: Evidence for the thermal dissociation of methane hydrate during the Paleocene-Eocene thermal maximum. Geology, 30: 1067-1070.

Thomas, E., 1998. Biogeography of the late Paleocene benthic foraminiferal extinction. In: M.P. Aubry, W.A. Berggren, S. Lucas (Editors), Late Paleocene-Early Eocene

BIotic and Climatic Events in the Marine and Terrestrial Records. Columbia University Press, New York, pp. 214-243.

Tripati, A.K., Elderfield, H., 2004. Abrupt hydrographic changes in the equatorial Pacific and subtropical Atlantic from foraminiferal Mg/Ca indicate greenhouse origin for the thermal maximum at the Paleocene-Eocene Boundary. Geochemistry Geophysics Geosystems, 5.

Ward, J.K., Harris, J.M., Cerling, T.E., Wiedenhoeft, A., Lott, M.J., Dearing, M.D., Coltrain, J.B., Ehleringer, J.R., 2005. Carbon starvation in glacial trees recovered from the La Brea tar pits, southern California. Proceedings of the National Academy of Sciences of the United States of America, 102: 690-694.

Wing, S.L., 1998. Late Paleocene-Early Eocene floral and climatic change in the Bighorn Basin, Wyoming. In: M.P. Aubry, W.A. Berggren, S. Lucas (Editors), Late Paleocene-Early Ecoene Biotic and Climatic Events. Columbia University Press, New York, pp. 371-391.

Wing, S.L., Alroy, J., Hickey, L.J., 1995. Plant and mammal diversity in the Paleocene to early Eocene of the Bighorn Basin. Palaeogeography Palaeoclimatology Palaeoecology, 115: 117-156.

Wing, S.L., Harrington, G.J., Smith, F.A., Bloch, J.I., Boyer, D.M., Freeman, K.H., 2005. Transient floral change and rapid global warming at the Paleocene-Eocene boundary. Science, 310: 993-996.

Zachos, J.C., Rohl, U., Schellenberg, S.A., Sluijs, A., Hodell, D.A., Kelly, D.C., Thomas, E., Nicolo, M., Raffi, I., Lourens, L.J., McCarren, H., Kroon, D., 2005. Rapid acidification of the ocean during the Paleocene-Eocene thermal maximum. Science, 308: 1611-1615.

Zachos, J.C., Shouten, S., Bohaty, S., Quattlebaum, T., Sluijs, A., Brinkhuis, H., Gibbs, S.J., Bralower, T.J., 2006. Extreme warming of mid-latitude coastal ocean during the Paleocene-Eocene Thermal Maximum: Inferences from TEX_{86} and isotope data. Geology, 34: 737-740.

Zachos, J.C., Wara, M.W., Bohaty, S., Delaney, M.L., Petrizzo, M.R., Brill, A., Bralower, T.J., Premoli-Silva, I., 2003. A transient rise in tropical sea surface temperature during the Paleocene-Eocene Thermal Maximum. Science, 302: 1551-1554.